Bai *et al. Cell Communication and Signaling* (2025) 23:217
https://doi.org/10.1186/s12964-025-02217-9

Cell Communication and Signaling

RESEARCH Open Access

Accumulation of long-chain unsaturated fatty acids in the airway inflammatory microenvironment drives eosinophil etosis and corticosteroid resistance

Yurong Bai[1,2,3†], Pengda Fang[1,2,3†], Shasha Li[4,5,6†], Zhenhao Xiao[1,2,3†], Wenyi Chen[1,2,3], Wenlong Li[1,2,3], Xinyue Wang[1,2,3], Jingyuan Chen[1,2,3], Yue Li[1,2,3], Junhai Chen[1,2,3], Weiqiang Huang[1,2,3], Xin Luo[1,2,3], Shigeharu Ueki[7], Deyu Fang[8], Qintai Yang[1,2,3*] and Yana Zhang[1,2,3*]

Abstract

Background Eosinophilic inflammation is a feature of chronic rhinosinusitis with nasal polyps (CRSwNP). Patients with eosinophilic CRSwNP (ENP) tend to be refractory and prone to recurrence. Although there is increasing evidence linking lipid metabolic irregularities to eosinophilia, the particular lipid responsible for promoting eosinophilic inflammation and the precise molecular mechanisms involved remain unclear.

Methods Lipidomic atlas and metabolic pathway enrichment were identified by liquid chromatography-tandem mass spectrometry and RNA sequencing, respectively. Eosinophil extracellular trap cell death (EETosis) was detected by immunofluorescence microscopy and transmission electron microscopy. Functional analyses were performed on purified eosinophils.

Results The unbiased lipidomic atlas identified a specific accumulation in long-chain fatty acids (LCFAs) in ENP. Consistently, RNA-seq analysis confirmed the enrichment in long-chain unsaturated fatty acid metabolism pathway in ENP. In this lipid-rich airway inflammatory environment, EETosis including ETotic eosinophils, EETs release and Charcot-Leyden crystals (CLCs) generation was enhanced in ENP, and associated with disease severity. Further, we found that both saturated and unsaturated LCFAs, such as arachidonic acid, are critical fuel sources to trigger eosinophil activation and filamentous DNA release, whereas only arachidonic acid could induce crystalline Galectin10 (CLCs). Mechanistically, arachidonic acid induces EETosis through a mechanism independent of reactive oxygen species but the IRE1α/XBP1s/PAD4 pathway. Both the long-acting dexamethasone and short-acting hydrocortisone, while facilitate eosinophil apoptosis, are ineffective to block arachidonic acid-induced EETosis.

†Yurong Bai, Pengda Fang, Shasha Li and Zhenhao Xiao equally contributed to this work.

*Correspondence:
Qintai Yang
Yangqint@mail.sysu.edu.cn
Yana Zhang
Zhangyn95@mail.sysu.edu.cn

Full list of author information is available at the end of the article

Conclusions Our findings demonstrate a previously unknown role of the LCFA arachidonic acid in mediating EETosis and glucocorticoid insensitivity to drive ENP progression, which may lead to novel insights regarding the treatment of patients with refractory eosinophilic inflammation.

Keywords Eosinophil extracellular trap cell death, Long-chain fatty acids, Endoplasmic reticulum, Protein arginine deiminase 4, Glucocorticoid insensitivity

Introduction

Chronic rhinosinusitis with nasal polyps (CRSwNP) is a multifactorial disease of the upper airways with a high prevalence, and it remains a significant public health problem with a considerable socioeconomic burden [1]. Around 80% white CRSwNP patients and 40% Asian CRSwNP patients have been characterized as eosinophilic inflammation [2]. Patients with eosinophilic CRSwNP (ENP) exhibit more severe symptoms, poorer clinical control, and higher risk of recurrence than patients with non- eosinophilic CRSwNP (nENP) [3, 4], implying that eosinophils play a central role in the progression and prognosis of CRSwNP.

Eosinophils must undergo receptor-mediated activation to cause tissue damage [5]. Recent studies have shed light on active cytolytic eosinophil death, called eosinophil extracellular trap cell death (EETosis), which releases eosinophil extracellular DNA traps (EETs), Charcot-Leyden crystals (CLCs), and total cellular contents after hyperactivation [3, 6, 7]. EETs have been associated with CRSwNP endotypes, severity and refractoriness [8–12]. The pathological contribution of EETosis is made more convincing by CLCs. Studies from us and others have demonstrated that CLCs are served as a potential biomarker for predicting CRSwNP recurrence and steroid sensitivity [13, 14]. Although EETosis is closely associated with progression, refractoriness, and prognosis in type 2 inflammation, how EETosis occurs in the upper airway inflammatory microenvironment remains obscure.

Recent research unraveled that nasal polyp-derived eosinophils possess a specific phenotype with dysregulated fatty acid metabolism [15], suggesting that the metabolic state may be among the main contributing determinants of the activation and function of eosinophils. In addition, an augmented unsaturated fatty acids oxidation was positively correlated with mucosal eosinophilia [16, 17]. These findings suggest that eosinophil infiltration may be intertwined with lipid metabolic reprogramming. However, it remains largely unclear whether and how lipids deposited in nasal polyps (NPs) sophisticatedly orchestrate eosinophil activation.

The treatment of CRSwNP, surgically or with medicine or both, forms a dilemma due to the high recurrence rate. Compelling clinical evidence has demonstrated that topical glucocorticoids (GCs) have potent effects on eosinophilic inflammation [18]. However, the high recurrence rate of ENP implies that certain substances in eosinophils are ineffective to GCs and they may lurk in the airway microenvironment, thus maintain long-term inflammation as well as initiate recurrence.

The aim of this study was to uncover lipidomic atlas in nasal polyps and to investigate the unappreciated contributions of accumulated lipids to EETosis and GC's insensitivity.

Methods

Subjects

This study was approved by the Ethics Committee of The Third Affiliated Hospital of Sun Yat-sen University (II2023-117-01), and conducted with written informed consent from all subjects. Diagnosis of CRSwNP was according to the European Position Paper on Rhinosinusitis and Nasal Polyps (EPOS) 2012 [19]. NP tissues from middle meatus were collected during surgery. ENP was defined when the percentage of tissue eosinophils ≥ 10% of total inflammatory cells [20]. Control subjects were patients undergoing septoplasty because of anatomic variations without sinonasal diseases. A single biopsy was obtained from the inferior turbinate (IT) mucosa of each control patient during septoplasty. Freshly obtained nasal biopsies were divided into 2 parts. One part was fixed in formaldehyde solution for histopathology, and the other part was immediately snap frozen in liquid nitrogen and stored at − 80 °C for later quantitative RT-PCR, lipidomic analysis or RNA sequencing. The detailed demographic characteristics are provided in Table E1. All the subjects were enrolled with strict inclusion and exclusion criteria as described in the online supplementary file.

Lipidomic analysis

Untargeted liquid chromatography-tandem mass spectrometry (LC-MS/MS) lipidomic analyses were performed on sinonasal biopsies (IT, ENP, and nENP) as previously reported [21]. The lipid classification and function enrichment analysis were performed with a web-based tool of lipid ontology (LION) [22]. The detailed information is listed in the online supplementary file.

RNA sequencing and data analysis

Total RNA was extracted from sinonasal tissues (IT, ENP, and nENP) using TRIzol (TaKaRa Biotechnology). RNA sequencing was performed on the Illumina Novaseq 6000 platform. Pathways enrichment analysis was performed

by using the gene set enrichment analysis (GSEA). More information is provided in the online supplement.

Immunofluorescence microscopy and transmission electron microscopy

Tissue sections/eosinophil coverslips were incubated with specific primary antibody overnight at 4℃ followed by incubation with corresponding secondary antibody for 1 h at room temperature. Hoechst 33342 (Hoe, Invitrogen) was used to counterstain of nuclei. A summary of antibodies used is provided in Table E2. The morphology of CLCs was also detected using transmission electron microscope (Philips) at 60KV [3]. More information is provided in the online supplement.

Lipid staining

Histologic visualization of neutral fat in nasal tissues (IT, ENP, and nENP) was evaluated using the Oil Red O kit (Beyotime) [23]. Briefly, frozen sinonasal sections were placed in propylene glycol for 2 min and stained with Oil Red O Solution for 20 min, and counterstained with hematoxylin.

Quantitative RT-PCR

Total RNA was extracted from samples using TRIzol [24]. A total of 1 μg RNA was employed to synthesize cDNA and PCR was performed by using TB Green master mix kit (TAKARA Biotechnology) with specific primers listed on Table E3.

Isolation of peripheral blood eosinophils

Eosinophils from human peripheral blood were isolated using the Eosinophil Isolation Kit (Miltenyi Biotec) [25]. Isolated eosinophils with purity > 95% and viability > 98%, as evidenced by flow cytometry and immunofluorescence staining, were used for further experiments.

Induction and measurements of EETs/CLCs in vitro

Purified eosinophils (2.0×10^5cells) were cultured with RPMI 1640 media containing 0.3% BSA in 24 well chambered coverglass. Eosinophils were treated with palmitic acid (PA), oleic acid (OA), arachidonic acid (AA), and/or house dust mite (HDM, Greer) as well as corresponding vehicle for 3 h to induce EETs/CLCs in the presence or absence of diphenyleneiodonium chloride (DPI, Sigma), and BBCl (MCE). Phorbol 12-myristate 13-acetate (PMA; Sigma) was used as the positive control. At the end of induction, Sytox Green (Invitrogen) was applied to evaluate EETs. Mitotracker Red CMXRos (Invitrogen) was used to test the presence of mitochondrial DNA.

Measurement of reactive oxygen species production

Reactive oxygen species (ROS) production in treated eosinophils was measured by 2', 7'-Dichlorofluorescin diacetate (H_2DCFDA, Sigma) and evaluated using fluorescence microscopy.

Endoplasmic reticulum (ER) stress Inhibition

For mechanistic studies, eosinophils were pretreated with tauroursodeoxycholic acid (TUDCA, TargetMol), MKC8866 (Selleck), and responding vehicle for 30 min, respectively. Then, eosinophils were restimulated with AA in presence of TUDCA/MKC8866, followed by morphological detection of EETs and CLCs.

Western blotting

Total protein was extracted from treated eosinophils and 40 μg proteins were separated by 10% sodiumdodecyl sulfate-polyacrylamide gel electrophoresis and transferred to polyvinylidene fluoride membrane (PVDF, Merck Millipore). The membranes were blocked with 5% fat-free skim milk for 1 h, and then incubated overnight with primary antibodies as listed in Table E4.

Apoptosis evaluation

TMR Tunnel Cell Apoptosis Detection Kit (Servicebio) was used to identify apoptotic eosinophils under the condition of AA stimulation in presence or absence of dexamethasone/hydrocortisone.

ELISA assay

Gal10 protein was detected from supernatants using anti-Gal10 kit (Cloud-clone) according to the manufacturer's instruction. Absorbance was measured at a wavelength of 450 nm with a microplate reader.

Additional methods are presented in the online supplementary file.

Statistical analyses

Statistical analysis was performed with SPSS 20.0 software. For continuous variables data, Kruskal-Wallis *H* test was used for significant intergroup variability. The Mann-Whitney *U* test was used for between-group comparison. Spearman test was performed for correlation analysis. Cell culture data were analyzed using unpaired Students' t-test or one-way ANOVA. *P* values < 0.05 were considered significant.

Results

The lipidomic atlas identified accumulation of long-chain fatty acids (LCFAs) in the inflammatory microenvironment of ENP

Sinonasal biopsies from 12 control subjects, 8 nENP and 11 ENP patients were subjected to untargeted lipidomics (Fig. 1A). An unsupervised principal component analysis (PCA) revealed that three distinct clusters of lipidomic profiles among these 31 subjects (Fig. 1B). Consensus clustering analysis showed obvious discrimination in

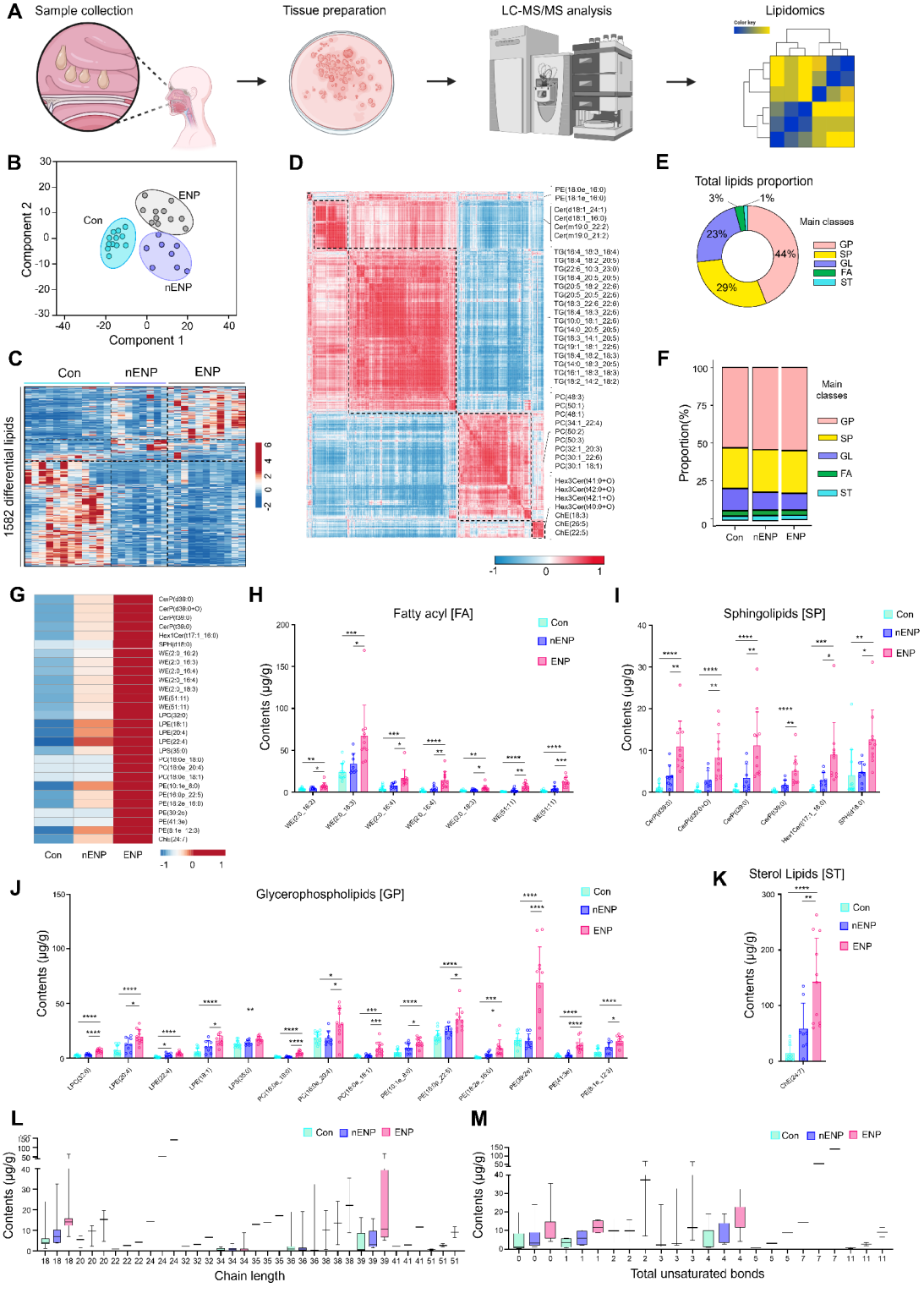

Fig. 1 (See legend on next page.)

(See figure on previous page.)

Fig. 1 Accumulation of long-chain fatty acids in ENP revealed by lipidomics. Inferior turbinate (IT) tissue from controls ($n=12$), NPs from patients with ENP ($n=11$) and nENP ($n=8$) were underwent LC-MS/MS. (**A**) Schematic illustration of untargeted LC-MS/MS based on lipidomics from sinonasal tissues. (**B**) Principal component analysis (PCA) of identified sinonasal tissues from controls, and patients with nENP and patients with ENP. (**C**) Unsupervised clustering analysis of the differentially expressed lipid molecules in control, nENP and ENP. 1, 582 differentially expressed lipids were used to plot the heatmap. Color code indicated in the legend. (**D**) Heatmap showing the correlation between each differential lipid as measured by Spearman's correlations. Color code indicated in the legend. (**E**) The proportion of main classes of differential lipids (glycerophospholipids, GP; sphingolipids, SP; glycerolipids, GL; fatty acyls, FA; and sterol lipids, ST). (**F**) Bar graph showing the proportion of five lipid classes from sinonasal mucosa in the three groups; (**G**) Heatmap showing the 28 significantly upregulated lipids in ENP. See legend for color code. (**H-K**) Bar graph showing the absolute quantitative statistics of 28 lipid molecules with significant differences in FA (**H**), SP (**I**), GP (**J**) and ST (**K**) main classes separately. (**L-M**) Statistical analysis of chain length (**L**) and unsaturated bond (**M**) of 28 lipid molecules with significant differences. For statistical analysis, one-way ANOVA followed by Tukey's post-hoc test was performed. $^{*}P<0.05$; $^{**}P<0.01$; $^{***}P<0.001$; $^{****}P<0.0001$

samples among three groups (Figure S1A). A total of 4, 703 unique lipids were identified in the sinonasal tissues from ENP, nENP and controls. Clustering analysis of the differential expressed lipids showed clear discrimination in lipid composition among ENP, nENP and controls (Fig. 1C). Likewise, the correlation analysis further demonstrated that differential lipids from the same subclass were positively correlated (Fig. 1D).

According to the LIPID MAPS structure database, five main classes of the identified lipids were uncovered: glycerophospholipids (GP, 44%), sphingolipids (SP, 29%), glycerolipids (GL, 23%), fatty acyls (FA, 3%) and sterol lipids (ST, 1%) (Fig. 1E). Next, the volcano plots displaying differentially expressed lipid classes and overall lipid atlas were presented among three groups (Figure S1B-D). The proportion of each class was comparable among these three groups (Fig. 1F). After removing those with the variable importance for the projection (VIP) less than 1, 28 enriched lipids including WE (2:0_16:3), PC (16:0e_18:0), PE (16:0p_22:5), CerP (39:0), and ChE (24:7) were identified in ENP group (Fig. 1G-K).

Interestingly, we found that fatty acids with carbon chain length of 18 ~ 51 carbons and with unsaturated carbon bonds were mainly enriched in ENP (Fig. 1L&M). Collectively, lipidomic analysis demonstrates that LCFAs with different unsaturated bonds are abundantly present in ENP, which suggesting that LCFAs may fuel the metabolic needs of infiltrating eosinophils.

Enriched long-chain unsaturated fatty acid metabolism pathway in ENP

To further ascertain the enriched metabolic pathways in ENP, RNA-seq was applied. The cellular metabolic processes including carbohydrate metabolism, nucleotide metabolism, amino acid metabolism, electron transport chain (ETC), and lipid metabolism were present in sinonasal biopsies (Fig. 2A). Interestingly, lipid metabolism is the most enriched metabolic modality in ENP relative to nENP and control (Fig. 2A). Further analysis of lipid metabolism pathway showed that fatty acid biosynthetic/metabolic process, long-chain/unsaturated fatty acid metabolic process, and arachidonic acid (AA) metabolic process were significantly upregulated in ENP (Fig. 2B). GSEA also exhibited the enrichment of lipid metabolism pathways, especially the AA metabolism, in ENP (Fig. 2C). In addition, RNA-seq and PCR analysis demonstrated that LCFA/AA metabolism associated genes such as *ALOX15*, arachidonate 5-lipoxygenase activating protein (*ALOX5AP*), hematopoietic prostaglandin D synthase (*HPGDS*), and ELOVL fatty acid elongase 5 (*ELOVL5*) were increased in ENP (Fig. 2D&E).

LCFAs usually form lipid droplets (LDs) to supply energy for cell homeostasis. We found that LD deposition was increased in ENP when compared with nENP and control (Figure S2A&B). Intriguingly, the LDs were predominantly concentrated within eosinophils and were correlated with eosinophil count (Figure S2A-D). Moreover, RNA-seq data showed that eosinophil activation positively correlated with long-chain/unsaturated fatty acid/AA metabolism and associated genes such as *ALOX15* and *ALOX5AP* (Fig. 2F). Thus, ENP is an inflammatory environment enriched with long-chain/unsaturated fatty acids, especially AA metabolism, which may trigger eosinophil activation.

Abundance of EETosis-derived extracellular DNA traps and CLCs in ENP

Although ETotic eosinophils and EETs structure have been shown in the bronchial mucous plugs and NPs [26], the sophisticated characteristics of EETs in NPs have not been fully elucidated. Citrullinated histone H3 (CitH3) is a central player in generating EETs, so immunofluorescence analysis of eosinophil cationic protein (ECP), CitH3 and Hoe were performed. We observed a strong co-localization of the decondensed thread-like DNA with ECP consist of filamentous CitH3 structures ($CitH3^{+}Hoe^{+}ECP^{+}$EETs) in ENP, and that tissue eosinophils releasing EETs exhibit cytolysis accompanied by disrupted plasma membrane, nuclear envelope, and extracellular granule (ECP) release (Fig. 3A). The enhanced web-like EETs were observed in ENP relative to nENP and controls (Fig. 3B-D). And EETs number strongly correlated with eosinophils number and disease severity (Fig. 3E-G). Consistent with previous research [3, 13, 27], increased CLCs, detected by H&E staining, immunofluorescence and transmission electron

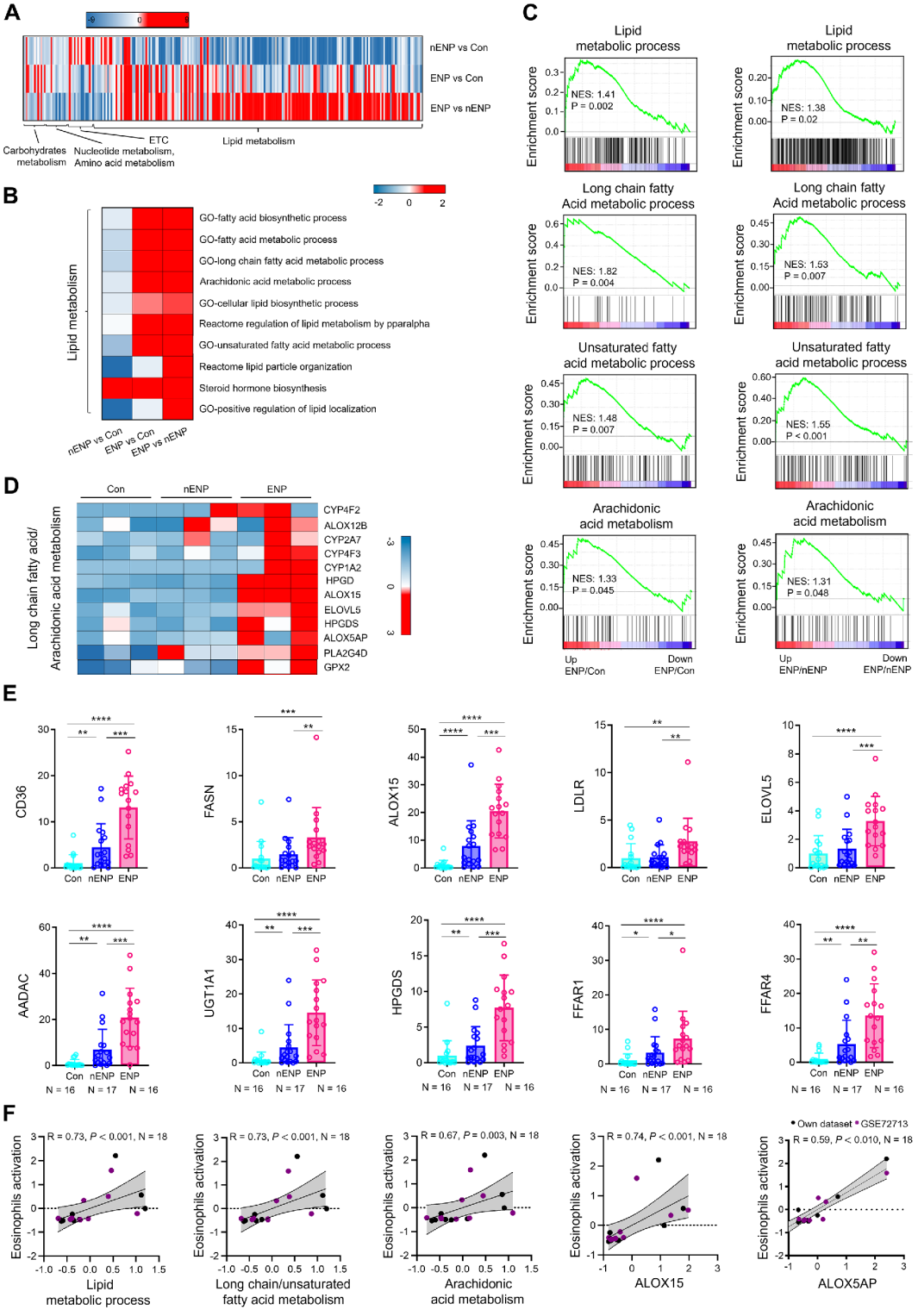

Fig. 2 (See legend on next page.)

(See figure on previous page.)

Fig. 2 Augmented long-chain fatty acid metabolism pathway in ENP. (**A-D**) Inferior turbinate (IT) tissue from controls ($n=3$), NPs from patients with ENP ($n=3$) and nENP ($n=3$) were undergone bulk RNA-seq. (**A**) Unsupervised clustering analysis of the different metabolic pathways in sinonasal tissues from the three groups. Color code indicated in the legend. (**B**) Heatmap showing fold changes of lipid metabolism pathways in sinonasal tissues from the three groups. Color code indicated in the legend. (**C**) GSEA plots showing enrichment scores for lipid metabolic process/long-chain fatty acid (LCFA) metabolic process/unsaturated fatty acid metabolic process/arachidonic acid metabolism in ENP/con and ENP/nENP. (**D**) Heatmap showing relative expression of LCFA/arachidonic acid metabolism genes in sinonasal mucosa from the three groups. Expression signals are depicted using pseudocoloring, in which expression for each gene is shown as high (red) or low (blue). (**E**) QPCR analysis of relative mRNA expression of LCFA/arachidonic acid metabolism genes including CD36, FASN, ALOX15, LDLR, ELOVL5, AADAC, UGT1A1, HPGDS, FFAR1 and FFAR4 in sinonasal mucosa from controls ($n=16$), NPs from patients with nENP ($n=17$) and ENP ($n=16$). For statistical analysis, 2-tailed Mann-Whitney U test was performed. (**F**) Correlation analysis of enrichment score (Z score) between eosinophils activation and lipid metabolic process, long-chain/unsaturated fatty acid metabolism, arachidonic acid metabolism, ALOX15 and ALOX5AP, respectively ($n=18$). Some data were extracted from GEO database (GSEA72713). R and *P* values were determined by a 2-tailed Spearman correlation test. *$P<0.05$; **$P<0.01$; ***$P<0.001$; ****$P<0.0001$

microscopy, was observed in ENP (Fig. 3H-K). The quantity of CLCs was positively correlated with VAS score and SNOT-22 score (Fig. 3L&M). Our data indicate that eosinophils in NPs experience EETosis and exacerbate disease severity by release EETs and CLCs.

LCFAs induce EETosis

Next, we aim to investigated whether human eosinophils experience EETosis in response to LCFAs in vitro. Isolated eosinophils with purity > 95% were incubated with different LCFAs including palmitic acid (PA), oleic acid (OA), and arachidonic acid (AA) (Fig. 4A & Figure S3A-C). EETs were released in a dose- and time- dependent manner (Figure S4&5). Confocal images indicated that eosinophils release nuclear contents as filamentous chromatin structures in presence of PA, OA, and AA (Fig. 4B-C). Interestingly, AA was more potent EETosis inducer than PA and OA, as indicated by the increased releasing EETs in AA- treated eosinophils compared to PA- and OA- stimulated eosinophils (Fig. 4C). We also found few mitochondria-derived extracellular traps during AA-induced EETosis (Fig. 4D), suggesting that AA-mediated EETs are mainly nuclear-derived chromatin fibers.

Moreover, we found that only AA treatment facilitated CLCs formation in the cytoplasm, although PA, OA, and AA stimulation could induce releasing Gal10 protein (Fig. 4E-G). These data indicate that the long-chain polyunsaturated fatty acid AA, rather than OA and PA, possesses potent capacity to promote Gal10 crystallization. Consistent with enhanced production of EETs and CLCs, protein levels of PAD4 and CitH3 were upregulated following AA treatment (Fig. 4H). Further, eosinophil granule proteins PRG2 and ECP were detected as punctate foci of 1–2 μm diameter in the DNA net (Fig. 4I). In addition, Gal10 protein, but not crystalline CLCs showed colocalization with PRG2 and ECP (Fig. 4J). Thus, the long-chain polyunsaturated fatty acid AA possesses potent capacity to facilitate EETosis.

House dust mite (HDM) augments AA-induced EETosis

Given that HDM can drive EETs release from mice eosinophils in vivo [28], we next explored whether antigen exposure exacerbates AA-induced EETosis. HDM, the most common allergen in CRS patients of southern China, was applied. We observed that HDM itself could drive EETs release, CLCs formation, and degranulation from human eosinophils in vitro (Fig. 5A-E). Moreover, enhanced EETs, CLCs, and CLC protein were observed in eosinophils incubated with HDM and AA relative to that in eosinophils stimulated with HDM or AA alone (Fig. 5A-E). Our data indicate that HDM and AA have a synergistic effect to amplify EETosis. Beyond AA, HDM could also enhance PA-induced EETosis, albeit with slightly weaker potency compared to AA (Figure S6A-G). The characteristics of HDM-induced EETs was able to trap substantial number of eosinophils, which is different from the features of EETs induced by LCFAs and PMA (Fig. 5F). HDM-induced CLCs showed no colocalization with granule protein PRG2 (Fig. 5G). These results indicate that HDM can amplify the LCFAs-induced EETosis, seemingly independent of the saturation level of fatty acid carbon bonds.

AA-induced EETosis is dependent on ER stress sensor IRE1α/XBP1s pathway

To unravel the molecular mechanisms underlying the AA-induced EETosis in the upper airway inflammatory microenvironment, the enrichment analysis for the upregulated lipids in ENP was performed by LION. LION analysis revealed that the functional terms are mainly related to ER in ENP compared to nENP and controls (Fig. 6A&B), implying that the ER stress signaling may modulate EETosis. This hypothesis was supported by RNA-seq data that ER stress was positively correlated with eosinophil activation (Fig. 6C). Although the critical function of ER stress sensor XBP1 on eosinophil differentiation has been addressed [29], whether IRE1α/XBP1 pathway modulates eosinophil activation and EETosis has been underrecognized. As expected, the protein levels of IRE1α and spliced-XBP1(XBP1s) were upregulated in eosinophils following AA stimulation (Fig. 6D). Moreover, AA-induced EETosis could be substantially blocked by MKC8866 (IRE1 RNase inhibitor) and TUDCA (ER stress inhibitor), as indicated by decreased EETs, CLCs,

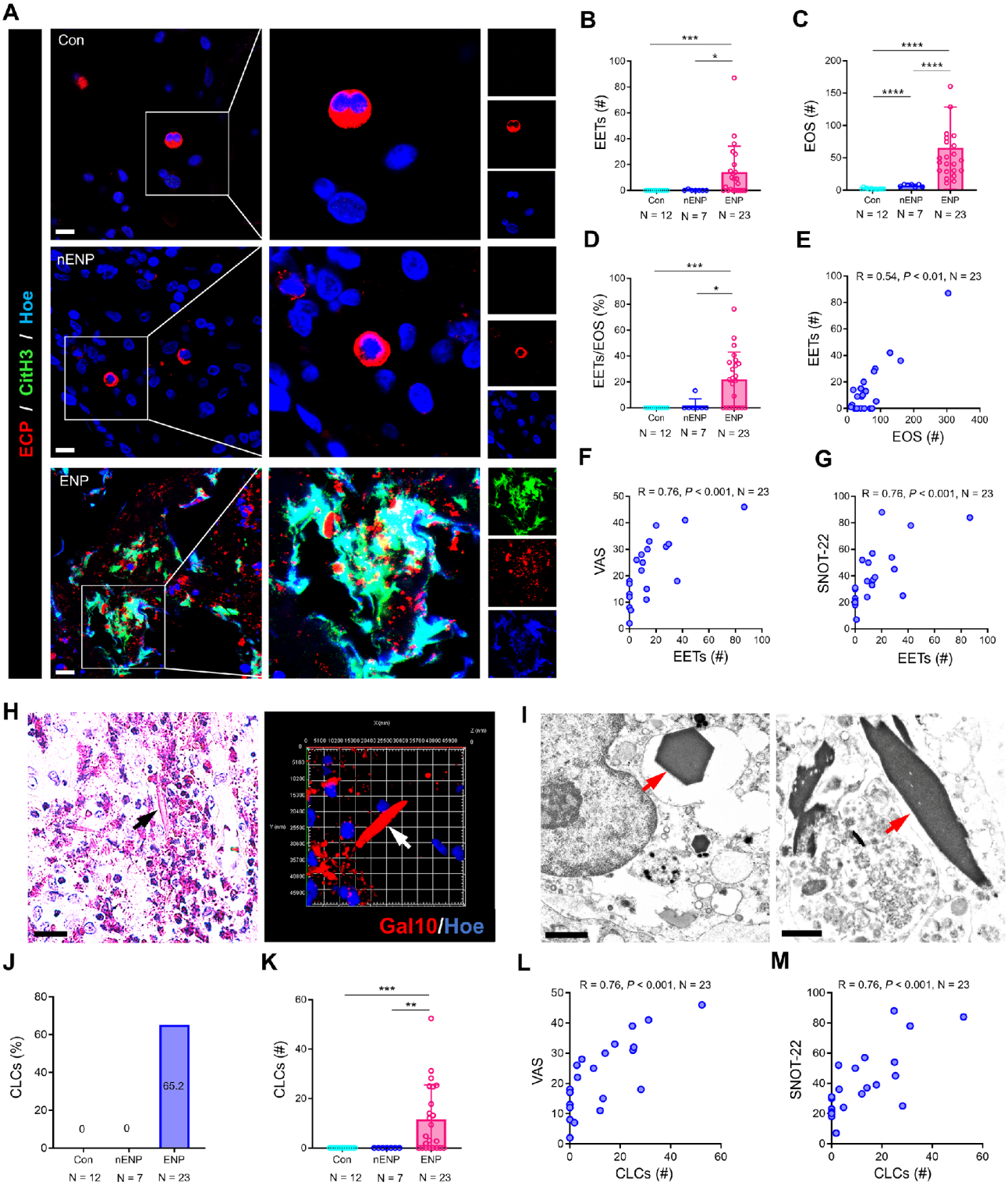

Fig. 3 (See legend on next page.)

(See figure on previous page.)

Fig. 3 Enriched EETosis-derived extracellular DNA traps and CLCs in ENP. (**A**) Confocal images of formalin-fixed, paraffin-embedded human sinonasal tissues displaying $ECP^+CitH3^+Hoe^+$EETs from control ($n=12$), nENP ($n=7$), and ENP ($n=23$) groups. ECP (red) and CitH3 (green) were detected by indirect immunofluorescence, and nuclei (blue) were stained with Hoechst 33342. Outlines show magnified views of representative subregions. Eosinophil with bilobed nuclei in controls (upper panel), eosinophils with a single round nuclei in nENP (middle panel); eosinophils with lytic nuclei in ENP (lower panel). Scale bar = 10 μm. Images are representative of one experiment in each group. (**B-D**) Quantitative analysis of EETs count (**B**), eosinophil count (**C**) and EETs percentage (**D**) in sinonasal tissues from the three groups (control, $n=12$; nENP, $n=7$; ENP, $n=23$). (**E-G**) Correlation analysis between EETs count and eosinophil count (**E**), VAS score (**F**), and SNOT-22 score (**G**), respectively ($n=23$). (**H**) Representative image of CLCs (arrowheads) by H&E staining (left panel, scale bar = 20 μm) and Gal10-Hoe immunofluorescence staining (right panel) of ENP from one CRSwNP patient. (**I**) Representative TEM image of bipyramidal hexagonal CLCs structure (arrowheads) of ENP from one CRSwNP patient. Scale bar = 1 μm. (**J-K**) Bar graph showing percentage (**J**) and quantitation (**J**) of CLCs in sinonasal tissue from control ($n=12$), nENP ($n=11$), and ENP ($n=23$) groups. (**L-M**) Correlation analysis between CLCs count and VAS score (**L**) and SNOT-22 score (M), respectively ($n=23$). (**B-D**) and (**K**), 2-tailed Mann-Whitney *U* test; (**E-G**) and (**L**&**M**), 2-tailed Spearman correlation test. $^*P<0.05$; $^{**}P<0.01$; $^{***}P<0.001$; $^{****}P<0.0001$

and degranulation (Fig. 6E-G). We also found that AA-induced enhancement of PAD4 and CitH3 were sufficiently repressed by MKC8866 and TUDCA (Fig. 6H), suggesting IRE1α/XBP1s is an upstream of PAD4 and CitH3, and exerts non-redundant function on AA-mediated EETosis.

Pioneering research has revealed the mechanisms for EETosis are involved with nicotinamide adenine dinucleotide phosphate (NADPH) and PAD4-mediated histone citrullination [3, 30]. Despite the remarkable reactive oxygen species (ROS) production (Figure S7), NADPH oxidase inhibitor DPI fail to blunt AA-induced EETosis. Whereas PAD4 inhibitor BBCl could largely suppress AA-induced EETosis (Fig. 6I-L), indicating that PAD4-mediated histone citrullination rather than NADPH is necessary for AA-induced EETosis. Collectively, we have identified a heretofore unknown role of IRE1α/XBP1s in AA-mediated EETosis, which involves the modulation of PAD4 and CitH3 expression.

Glucocorticoids are ineffective in impeding the AA-induced EETosis

GCs, as the mainstay of CRSwNP therapy, exert their therapeutic effects by promotion of eosinophil apoptosis. Therefore, we sought to investigate whether GCs could facilitate eosinophil apoptosis and inhibit EETosis in the context of AA stimulation. Long-acting dexamethasone and short-acting hydrocortisone were used in this study. Both dexamethasone and hydrocortisone could promote eosinophil apoptosis, as indicated by increased $TUNEL^+$ eosinophils following GCs treatment for 3 h (Figure S8A&B). Although the extensive ETotic eosinophils generation, AA treatment did not contribute to eosinophil apoptosis (Fig. 7A&B), suggesting that EETosis mediated by AA is independent on apoptosis. Further, we showed that dexamethasone and hydrocortisone facilitate eosinophil apoptosis but are ineffective to block EETosis under condition of AA stimulation for 3 h (Fig. 7C-F).

The effects of GCs on AA-induced EETosis were also evaluated following 24-hour stimulation. More apoptotic ($TUNEL^+$) cells were observed in eosinophils treated with 24-hour than those treated with3-hour (Figure S8C&D). AA treatment with 24 h partially impeded eosinophil apoptosis, which could be reversed by dexamethasone but not hydrocortisone (Fig. 7G&H). This possibly because that hydrocortisone has a shorter biologic half-life. Consistently, GCs treatment with 24 h were ineffective in blocking EETs release (Fig. 7I&J). These results imply that eosinophils stimulated with AA show compromised pro-apoptotic response, and GCs fail to block EETosis induced by AA.

Discussion

Our current study has uncovered a previously unappreciated function of LCFAs, especially AA, for inducing EETosis and GCs' ineffectiveness to suppress EETs and CLCs release and perpetuating eosinophilic airway inflammation. Mechanistically, AA facilitates EETosis depending on IRE1α-XBP1s-PAD4 pathway, which provided a potential therapeutic regimen for GCs-resistant eosinophilic inflammation.

Although pioneer study has described lipidomic profiling in sinus mucosa, some lipid species such as PS and PI were present below the detection limit due to technical limitations [31]. For the first time, we uncovered the lipidomic atlas of sinus mucosa from CRSwNP patients using untargeted absolute quantitative LC-MS/MS and found that long-chain unsaturated fatty acids were enriched in ENP. Furthermore, increased long-chain unsaturated fatty acids/AA metabolism pathways in ENP were confirmed by RNA-seq and PCR data. We also demonstrated that upregulated LDs are observed in ENP, and eosinophils are the main sources of LDs deposition, which implying that eosinophils could fuel airway inflammation even at times of nutrition restriction. Thus, we speculate that ENP stands for a lipid-enriched inflammatory microenvironment. Our hypothesis was supported by the elevated level of 15-oxo-eciosatetraenoic acid (15-oxo-ETE, AA metabolite) in NPs [32]. Higher levels of 15-oxo-ETE were observed in induced sputum supernatant from patients with Nonsteroidal anti-inflammatory drugs-exacerbated respiratory disease (N-ERD) than in those with aspirin-tolerant asthma (ATA) [33]. Consistently, N-ERD patients who responded to aspirin

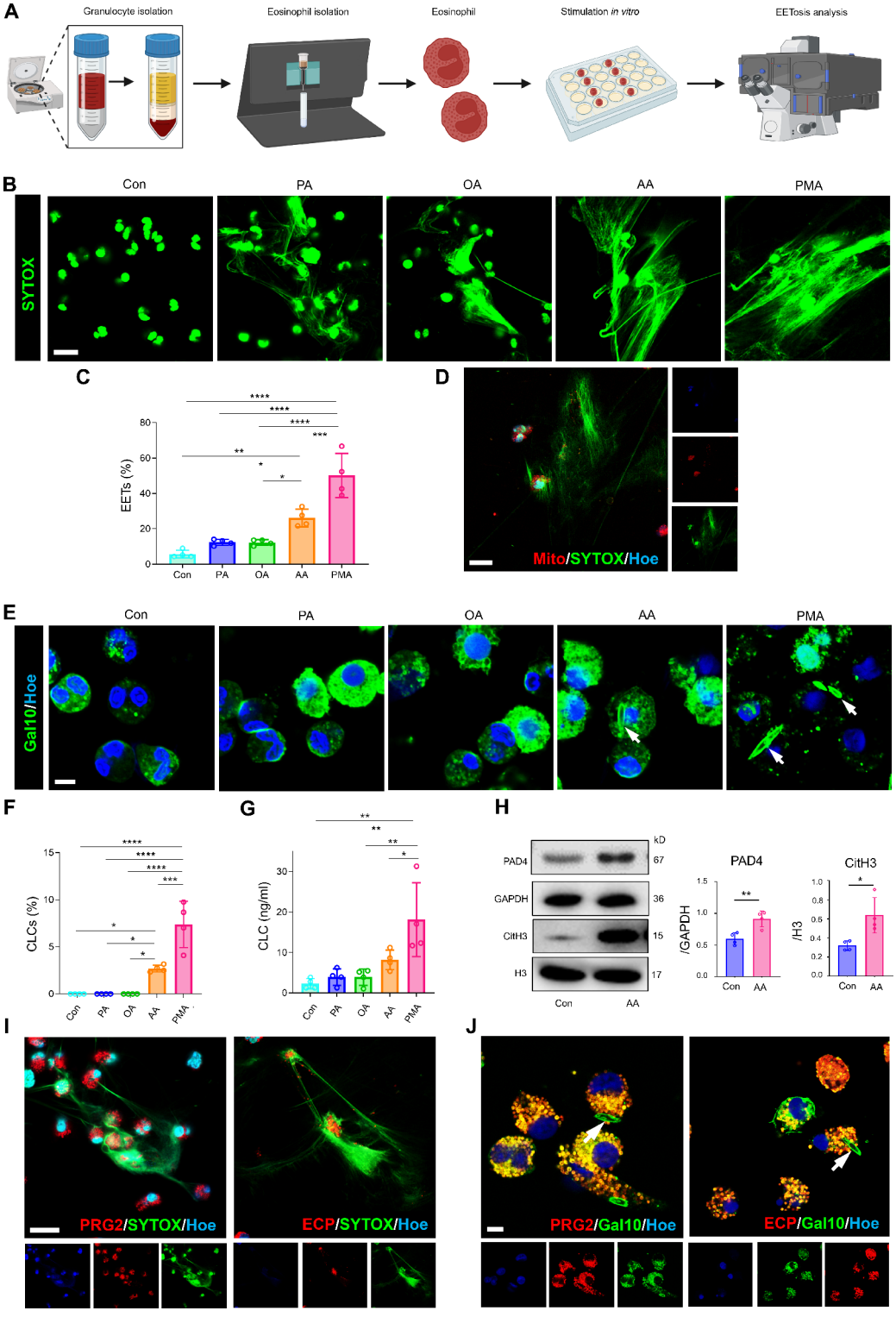

Fig. 4 (See legend on next page.)

(See figure on previous page.)

Fig. 4 Long-chain fatty acids drive EETosis generation. Human peripheral eosinophils were stimulated with long-chain fatty acids including palmitic acid (PA, 200μM), oleic acid (OA, 200μM), arachidonic acid (AA, 200μM), and corresponding vehicle for 3 h to induce EETs/CLCs formation. PMA (50 ng/mL) was used as the positive control. (**A**) Schematic representation of the experimental procedure. (**B**) Representative confocal images of EETs release from activated eosinophils with the indicated stimuli. Scale bar = 15 μm. (**C**) Percentage of EETs released from activated eosinophils with the indicated stimuli ($n = 4$). (**D**) Representative confocal image showing nuclear (SYTOX Green, green)- and mitochondria (MitoTracker, red)-derived EETs from AA-stimulated eosinophils. Nuclei (blue) were stained with Hoechst 33342. Scale bar = 15 μm. (**E**) Representative confocal image showing Gal10 (green)$^{+}$CLCs (arrowheads) production from activated eosinophils with the indicated stimuli. Nuclei are labeled blue with Hoechst 33342. Scale bar = 5 μm. (**F**) Percentage of CLCs production from activated eosinophils with the indicated stimuli ($n = 4$). (**G**) ELISA analysis showing quantification of CLC protein in supernatants from activated eosinophils with the indicated stimuli ($n = 4$). (**H**) Immunoblot analysis for PAD4 and CitH3 in eosinophils with or without AA stimulation ($n = 4$). (**I**) Representative confocal image showing colocalization of EETs (green) with intact granule PRG2 (red, left panel) and ECP (red, right panel) from eosinophils treated with AA. Scale bar = 15 μm. (**J**) Representative confocal image showing colocalization of CLCs (green) with intact granule PRG2 (red, left panel) and ECP (red, right panel) from eosinophils treated with AA. Scale bar = 5 μm. (**C**) and (**F**&**G**), 2-tailed one-way ANOVA; (**H**), 2-tailed unpaired t test. *$P < 0.05$; **$P < 0.01$; ***$P < 0.001$; ****$P < 0.0001$

therapy had a high baseline genetic expression of the *HPGD* (an enzyme required for 15-oxo-ETE synthesis) in sputum cells [34]. In addition, plasma levels of 15-oxo-ETE, but not urinary levels, were elevated in N-ERD patients compared to ATA and control groups [35], suggesting its potential as a diagnostic biomarker despite limited sensitivity. However, a ratio of urinary LTE4 to 15-oxo-ETE, corrected for sex and severity of CRSwNP, could be utilized as a non-invasive diagnostic tool for NERD [35]. Although elevated levels of 15-oxo-ETE in sputum, plasma, or urine may indicate an AA-enriched inflammatory microenvironment, whether such elevated levels are observed in patients with ENP and correlated with specific inflammatory cellular profiles requires further investigation. Recently, ENP has exhibited enhanced unsaturated fatty acid oxidization to facilitate mucosal eosinophilia by promoting eotaxin-3 expression [16, 36]. These studies suggest that long-chain unsaturated fatty acids in the context of airway inflammation are associated with eosinophil infiltration.

An array of evidence demonstrates that a variety of stimuli including PMA, platelet activating factor (PAF), the calcium ionophore A23187, *Aspergillus fumigatus*, and *Staphylococcus aureus* could mediate EETosis [6]. In the present study, we showed that LCFAs including AA, PA, and OA enable to mediate EETs release and degranulation, but only AA induces crystalline CLCs, implying that LCFAs with different saturation levels may exhibit heterogeneity in promoting eosinophil activation. AA may possibly possess a stronger capability to induce EETosis and perpetuate eosinophilic airway inflammation compared to OA and PA. Interestingly, HDM allergen could augment AA/PA induced EETosis. These results suggest that metabolic imbalance and environment stimuli may have a synergistic effect on driving airway inflammation.

The classical mechanisms of EETosis have been associated with NADPH oxidase (NOX)-dependent fashion. Recently, accumulating evidence that NOX-independent mechanisms has emerged [6, 37, 38]. EETs generation mediated by A23187-activated platelets was NOX-independent and was blocked by necroptosis inhibitors [37]. Whereas *Aspergillus fumigatus*- and lysophosphatidylserine-induced EETosis was dependent on CD11b and PAD4, respectively [26]. For the first time, we identified that IRE1α/XBP1s rather than NOX serves non-redundant functions to mediate EETosis by modulating PAD4 expression and histone citrullination. Heightened ER stress has been associated with severe eosinophilic in asthma and CRSwNP [39, 40]. IRE1α signaling is the most phylogenetically conserved branch of the ER stress response and the best studied in terms of its intersection with inflammatory pathways [41]. However, little was known about IRE1α in eosinophils prior a study in 2015 that linked ER stress to eosinophil differentiation [29]. The current study identified IRE1α/XBP1s as a critical upstream of PAD4 in AA-induced EETosis. Furthermore, the pathogenic function of IRE1α in eosinophils has been uncovered that pharmacological inhibition of IRE1α potentially suppress EETosis by downregulation of PAD4 and histone citrullination, highlighting therapeutic function of IRE1α inhibition for neutralizing EETosis in CRSwNP, and potentially other inflammatory conditions.

Synthetic GCs remain a first-line therapy for eosinophilic inflammation due to their potent anti-inflammatory effects [42]. Previous studies from us and others demonstrated that patients with CRSwNP exhibit GCs-resistance, which attributes to neutrophilia, IL-17 A-induced pyroptosis, and decreased mucin 1 level [43–45]. While eosinophilic inflammation is hypersensitive to GCs, which inhibit eosinophils survival and facilitate their apoptosis. Consistent with previous study, we found that GCs are able to induce eosinophil apoptosis. Contrary to our expectations based on the available literature, GCs could not suppress EETs release and CLCs production from AA-activated eosinophils. These results implying that GCs only could inhibit low-grade eosinophilic inflammation (cell number/quiescent eosinophils) but are ineffective in suppressing high-grade eosinophilic inflammation (EETosis/activated eosinophils). This phenomenon may explain why GCs can control eosinophilic inflammation but fail to inhibit eosinophilic NP recurrence (98.5% ENPs were recurrent after a 2-year follow-up[4]). Similar study on contact dermatitis demonstrated

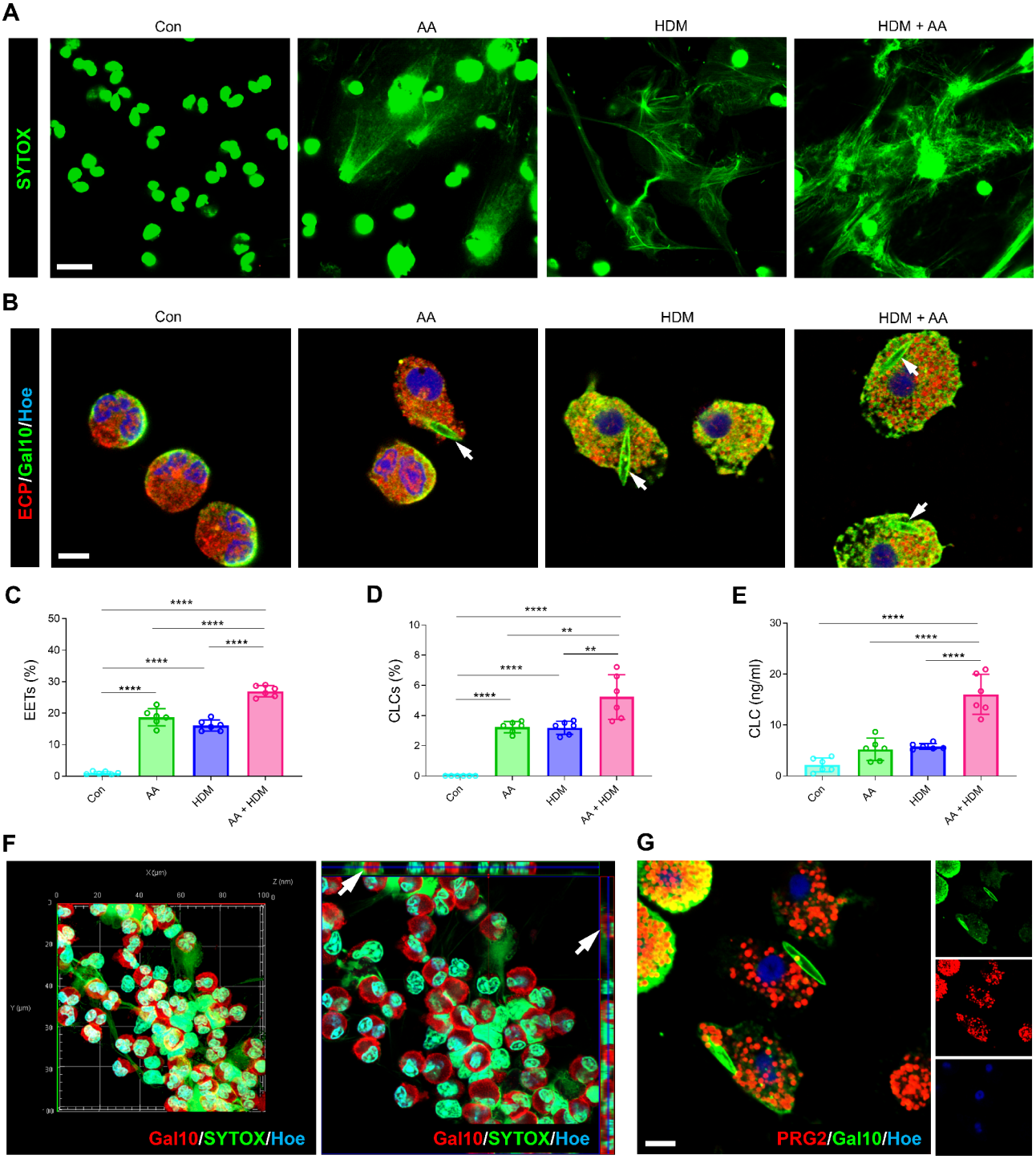

Fig. 5 HDM augments arachidonic acid-induced EETosis generation. Human peripheral eosinophils were stimulated with arachidonic acid (200μM) and/or HDM (20 μg/mL) and corresponding vehicle for 3 h to induce EETs/CLCs formation. (**A&B**) Representative confocal images of EETs release (A) and CLCs production (B, arrowheads) from activated eosinophils with the indicated stimuli. Scale bar = 15 μm (A); Scale bar = 5 μm (B). (**C**) Percentage of EETs released from activated eosinophils with the indicated stimuli ($n = 6$). (**D**) Percentage of CLCs production from activated eosinophils with the indicated stimuli ($n = 6$). (**E**) ELISA analysis showing quantification of CLC protein in supernatants from activated eosinophils with the indicated stimuli ($n = 6$). (**F**) Three-dimensional (left panel) and orthogonal (right panel) confocal image of EETs eructation from HDM-treated eosinophils. Arrowhead indicates $Gal10^+$ eosinophils trapped by Sytox $green^+$ EETs. (**G**) Representative confocal image showing colocalization of $Gal10^+$CLCs (green) with intact granule PRG2 (red) from eosinophils treated with HDM. Scale bar = 5 μm. (**C-E**), 2-tailed one-way ANOVA. $^{**}P < 0.01$; $^{***}P < 0.001$; $^{****}P < 0.0001$

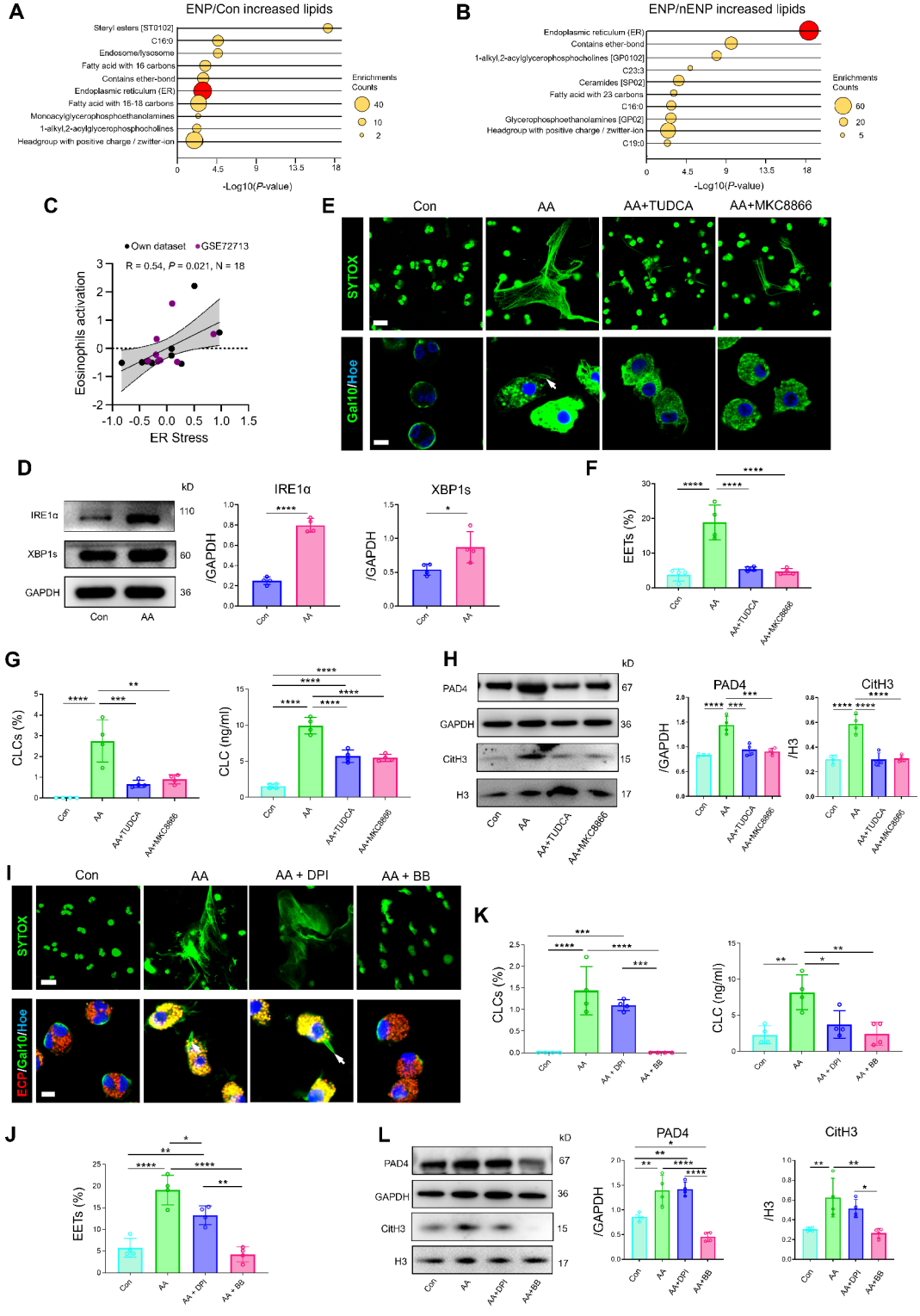

Fig. 6 (See legend on next page.)

(See figure on previous page.)

Fig. 6 Arachidonic acid-induced EETosis is dependent on IRE1α-XBP1s-PAD4 pathway. (**A&B**) Bubble plot showing the top 10 enriched functional pathways of significantly upregulated lipids in ENP compared to control (A) and to nENP (B) using lipid ontology (LION) enrichment analysis ($n=31$). (**C**) Correlation analysis of Z score between eosinophil activation and ER Stress ($n=18$). Data extracted from GSEA72713 are labeled with purple, and dataset generated in this study are labeled with black. (**D**) Immunoblot analysis for IRE1α and XBP1s in eosinophils with or without arachidonic acid stimulation ($n=4$). (**E**) Representative confocal images of EETs release (upper panel, scale bar = 15 μm) and CLCs production (arrowheads, lower panel, scale bar = 5 μm) from activated eosinophils with and without ER stress inhibitor (TUDCA, 50μM) and IRE1α RNase inhibitor (MKC8866, 10μM). (**F**) Percentage of EETs released from activated eosinophils with the indicated stimuli ($n=4$). (**G**) Percentage (left panel) of CLCs as well as CLC protein in supernatants (right panel) from activated eosinophils with the indicated stimuli ($n=4$). (**H**) Immunoblot analysis for PAD4 and CitH3 in eosinophils with the indicated stimuli ($n=4$). (**I**) Representative confocal images of EETs release (upper panel, scale bar = 15 μm) and CLCs production (arrowheads, lower panel, scale bar = 5 μm) from activated eosinophils with and without ROS inhibitor (DPI, 20μM) and PAD4 inhibitor (BBCI, 50 nM). (**J**) Quantification (left panel) and percentage (right panel) of EETs released from activated eosinophils with the indicated stimuli ($n=4$). (**K**) Percentage (left panel) of CLCs as well as CLC protein in supernatants (right panel) from activated eosinophils with the indicated stimuli ($n=4$). (**L**) Immunoblot analysis for PAD4 and CitH3 in eosinophils with the indicated stimuli ($n=4$). (**C**), 2-tailed Spearman correlation test; (**D**), 2-tailed unpaired t test; (**F-H**) and (**J-L**), 2-tailed one-way ANOVA. $^{*}P<0.05$; $^{**}P<0.01$; $^{***}P<0.001$; $^{****}P<0.0001$

that topical corticosteroids can inhibit allergic skin inflammation but are ineffective in impeding the formation and expansion of resident memory T cells [46]. Another study displayed that IL-5-activated eosinophils show impaired pro-apoptotic response to GCs, which may be mediated by the Nuclear Factor IL-3 [42]. This suggests that the effects of GCs on eosinophils may be affected by activation status. There are some limitations in the current study. First, the sample size in studies by bulk RNAseq is relatively small. However, the central conclusion was further validated by lipidomic analysis, qPCR, lipid staining and functional experiments. Future study should incorporate large cohorts with multicenter. Second, the underlying mechanisms by which GCs-insensitivity exhibited in AA-induced activated eosinophils warrants further study. Third, due to technical limitations, oxylipin contents of AA such as prostaglandins (PGDs), hydroxyeicosatetraenoic acids (HETES), and leukotrienes (LTs) could not be measured in the lipidomic dataset. However, elevated levels of both PGD2 and its metabolic product delta-12-PGD2 have been observed in ENP [16, 47]. Furthermore, elevated PGD2 levels in NPs are linked to eosinophil infiltration [47], and delta-12-PGD2 promotes eosinophil recruitment and activation through CRTH2 receptor activation [48]. In addition, increased levels of LTE4, PGD2, and 15(S)-HETE were observed in recurrent NP. These metabolites showed a positive correlation with eosinophil derived neutotoxin (EDN) in sinus secretions [49]. These results suggest that LTE4, PGD2, and 15(S)-HETE are strongly associated with eosinophil activation and may have the potential to induce EETosis.

In summary, our results show that LCFAs drive EETosis depends on IRE1α-XBP1s-PAD4 pathway, which contribute to GCs insensitivity and perpetuate airway inflammation. These findings expand our understanding of GCs' functions on eosinophilic inflammation, which may explain the reason that GCs' beneficial effects on suppress eosinophilic inflammation but ineffectiveness to block NP recurrence. Further, results from this study may provide the potential therapeutic target of IRE1α inhibition for neutralizing EETosis in CRSwNP, and potentially other eosinophils-dominated inflammatory conditions.

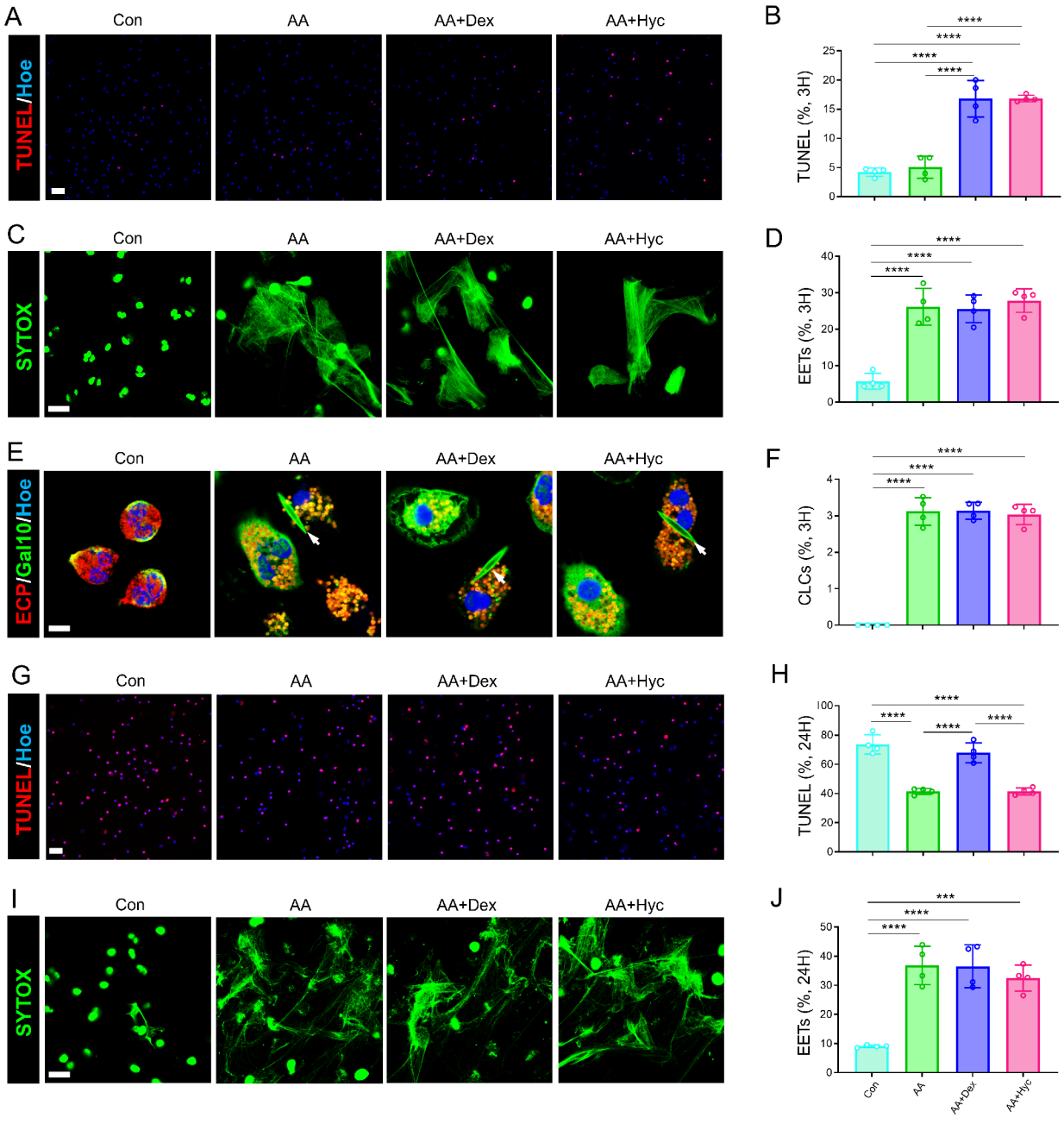

Fig. 7 Glucocorticoids (GCs) are ineffective in impeding arachidonic acid-induced EETosis generation. Human peripheral eosinophils were stimulated with arachidonic acid (AA, 200μM), AA plus dexamethasone (Dex, 0.4 mM; long-acting), AA plus hydrocortisone (Hyd, 0.2 mM; short-acting) and corresponding vehicle for 3 h and 24 h to induce EETs/CLCs formation, respectively. (**A**) Representative image showing TUNEL (red)$^+$cells in eosinophils with the indicated stimuli for 3 h. Nuclei are labeled blue with Hoechst 33342. Scale bar = 30 μm. (**B**) Percentage of TUNEL$^+$cells in eosinophils with the indicated stimuli for 3 h ($n = 4$). (**C**) Representative confocal images of EETs release from eosinophils treated with and without GCs for 3 h. Scale bar = 15 μm. (**D**) Percentage of EETs released from eosinophils treated with and without GCs for 3 h ($n = 4$). (**E**) Representative confocal images of Gal10$^+$CLCs production (arrowheads) from eosinophils treated with and without GCs for 3 h. Eosinophil granules are labeled red with anti-ECP antibody. Nuclei are labeled blue with Hoechst 33342. Scale bar = 5 μm. (**F**) Percentage of CLCs from eosinophils treated with and without GCs for 3 h ($n = 4$). (**G**) Representative image showing TUNEL (red)$^+$cells in eosinophils with the indicated stimuli for 24 h. Nuclei are labeled blue with Hoechst 33342. Scale bar = 30 μm. (**H**) Percentage of TUNEL$^+$cells in eosinophils with the indicated stimuli for 24 h ($n = 4$). (**I**) Representative confocal images of EETs release from eosinophils treated with and without GCs for 24 h. Scale bar = 15 μm. (**J**) Percentage of EETs released from eosinophils treated with and without GCs for 24 h ($n = 4$). (**B**, **D**, **F**, **H**, and **J**), 2-tailed one-way ANOVA. *$P < 0.05$; **$P < 0.01$; ***$P < 0.01$; ****$P < 0.0001$

Supplementary Information

The online version contains supplementary material available at https://doi.org/10.1186/s12964-025-02217-9.

Supplementary Material 1

Acknowledgements
The authors would like to thank YQW and QW (Zhongshan School of Medicine, Sun Yat-Sen University) for the assistance with transmission electron microscope and to thank Prof. GJS from the Third Affiliated Hospital of Sun Yat-Sen University for providing critical reagents.

Author contributions
YRB and PDF performed experiments, analyzed data, and wrote the manuscript. SSL performed experiments and analyzed data. ZHX, WYC, WLL, XYW, JYC, YL, JHC, WQH and XL assisted with collecting patient tissue samples and performed some experiments. DYF and SU gave constructive comments. YNZ and QTY designed the project and wrote the manuscript.

Funding
This work was supported by the National Natural Science Foundation of China (82371121, 82171114, 82271148), the Natural Science Foundation of Guangdong Province (2024A1515010052, 2022A1515011787), the Science and Technology Program of Guangzhou (202201020402, 2024A04J6570, 2023A03J0209), the Guangdong Provincial Pearl River Talents Program (0920220214), and the Key-area Research and Development Program of Guangdong Province (2020B0101130015).

Data availability
Data and code availability for the current study, please contact the corresponding author.

Declarations

Competing interests
The authors declare no competing interests.

Author details
[1]Department of Otolaryngology-Head and Neck Surgery, The Third Affiliated Hospital of Sun Yat-Sen University, No. 600 Tianhe Road, Guangdong, Guangzhou 510630, Guangdong, China
[2]Department of Allergy, The Third Affiliated Hospital of Sun Yat-Sen University, Guangzhou 510630, China
[3]Key Laboratory of Airway Inflammatory Disease Research and Innovative Technology Translation, Guangzhou 510630, China
[4]Department of Endocrinology and Metabolism, The Third Affiliated Hospital of Sun Yat-Sen University, Guangzhou 510630, China
[5]Guangdong Provincial Key Laboratory of Diabetology & Guangzhou Municipal Key Laboratory of Mechanistic and Translational Obesity Research, Guangzhou 510630, China
[6]Medical Center for Comprehensive Weight Control, The Third Affiliated Hospital of Sun Yat- Sen University, Guangzhou 510630, China
[7]Department of General Internal Medicine and Clinical Laboratory Medicine, Akita University Graduate School of Medicine, Akita 010-8543, Japan
[8]Department of Pathology, Northwestern University Feinberg School Medicine, Chicago, IL 60611, USA

Received: 7 February 2025 / Accepted: 25 April 2025
Published online: 07 May 2025

References

1. Fokkens WJ, Lund VJ, Hopkins C, Hellings PW, Kern R, Reitsma S, et al. European position paper on rhinosinusitis and nasal polyps 2020. Rhinology. 2020;58:1–464.
2. Yao Y, Zeng M, Liu Z. Revisiting Asian chronic rhinosinusitis in the era of type 2 biologics. Clin Exp Allergy. 2022;52:231–43.
3. Ueki S, Tokunaga T, Melo RCN, Saito H, Honda K, Fukuchi M, et al. Charcot-Leyden crystal formation is closely associated with eosinophil extracellular trap cell death. Blood. 2018;132:2183–7.
4. Lou H, Meng Y, Piao Y, Zhang N, Bachert C, Wang C, et al. Cellular phenotyping of chronic rhinosinusitis with nasal polyps. Rhinology. 2016;54:150–9.
5. Jesenak M, Diamant Z, Simon D, Tufvesson E, Seys SF, Mukherjee M, et al. Eosinophils-from cradle to grave: an EAACI task force paper on new molecular insights and clinical functions of eosinophils and the clinical effects of targeted eosinophil depletion. Allergy. 2023;78:3077–102.
6. Fukuchi M, Miyabe Y, Furutani C, Saga T, Moritoki Y, Yamada T, et al. How to detect eosinophil etosis (EETosis) and extracellular traps. Allergol Int. 2021;70:19–29.
7. Ueki S, Konno Y, Takeda M, Moritoki Y, Hirokawa M, Matsuwaki Y, et al. Eosinophil extracellular trap cell death-derived DNA traps: their presence in secretions and functional attributes. J Allergy Clin Immunol. 2016;137:258–67.
8. Hwang CS, Park SC, Cho HJ, Park DJ, Yoon JH, Kim CH. Eosinophil extracellular trap formation is closely associated with disease severity in chronic rhinosinusitis regardless of nasal polyp status. Sci Rep. 2019;9:8061.
9. Delemarre T, Holtappels G, De Ruyck N, Zhang N, Nauwynck H, Bachert C et al. A substantial neutrophilic inflammation as regular part of severe type 2 chronic rhinosinusitis with nasal polyps. J Allergy Clin Immunol 2021; 147:179– 88.e2.
10. Cha H, Lim HS, Park JA, Jo A, Ryu HT, Kim DW, et al. Effects of neutrophil and eosinophil extracellular trap formation on refractoriness in chronic rhinosinusitis with nasal polyps. Allergy Asthma Immunol Res. 2023;15:94–108.
11. Gevaert E, Zhang N, Krysko O, Lan F, Holtappels G, De Ruyck N, et al. Extracellular eosinophilic traps in association with Staphylococcus aureus at the site of epithelial barrier defects in patients with severe airway inflammation. J Allergy Clin Immunol. 2017;139:1849–e606.
12. Wang X, Sima Y, Zhao Y, Zhang N, Zheng M, Du K, et al. Endotypes of chronic rhinosinusitis based on inflammatory and remodeling factors. J Allergy Clin Immunol. 2023;151:458–68.
13. Chen W, Bai Y, Kong W, Luo X, Zeng Y, Chen J, et al. Predictive significance of Charcot-Leyden crystal structures for nasal polyp recurrence. Clin Transl Allergy. 2022;12:e12212.
14. Wu D, Yan B, Wang Y, Zhang L, Wang C. Charcot-Leyden crystal concentration in nasal secretions predicts clinical response to glucocorticoids in patients with chronic rhinosinusitis with nasal polyps. J Allergy Clin Immunol. 2019;144:345–e88.
15. Miyata J, Fukunaga K, Kawashima Y, Watanabe T, Saitoh A, Hirosaki T, et al. Dysregulated fatty acid metabolism in nasal polyp-derived eosinophils from patients with chronic rhinosinusitis. Allergy. 2019;74:1113–24.
16. Li JX, Wang ZZ, Zhai GT, Chen CL, Zhu KZ, Yu Z et al. Untargeted metabolomic profiling identifies disease-specific and outcome-related signatures in chronic rhinosinusitis. J Allergy Clin Immunol 2022; 150:727– 35.e6.
17. Ma Y, Wei Y, Liu X, Dang H, Zou H, Tian P, et al. Metabolomics analysis of metabolic patterns in chronic rhinosinusitis with nasal polyps. Allergy. 2022;77:653–6.
18. Watz H, Tetzlaff K, Wouters EF, Kirsten A, Magnussen H, Rodriguez-Roisin R, et al. Blood eosinophil count and exacerbations in severe chronic obstructive pulmonary disease after withdrawal of inhaled corticosteroids: a post-hoc analysis of the WISDOM trial. Lancet Respir Med. 2016;4:390–8.
19. Fokkens WJ, Lund VJ, Mullol J, Bachert C, Alobid I, Baroody F et al. European Position Paper on Rhinosinusitis and Nasal Polyps 2012. Rhinol Suppl. 2012; 23:3 p preceding table of contents, 1-298.
20. Cao PP, Li HB, Wang BF, Wang SB, You XJ, Cui YH et al. Distinct Immunopathologic characteristics of various types of chronic rhinosinusitis in adult Chinese. J Allergy Clin Immunol 2009; 124:478– 84, 84.e1-2.
21. Van Nevel S, Declercq J, Holtappels G, Lambrecht BN, Bachert C. Granulocyte-colony stimulating factor: missing link for stratification of type 2-high and type 2-low chronic rhinosinusitis patients. J Allergy Clin Immunol. 2022;149:1655–e655.
22. Molenaar MR, Jeucken A, Wassenaar TA, van de Lest CHA, Brouwers JF, Helms JB. LION/web: a web-based ontology enrichment tool for lipidomic data analysis. Gigascience 2019; 8.
23. Manzo T, Prentice BM, Anderson KG, Raman A, Schalck A, Codreanu GS et al. Accumulation of long-chain fatty acids in the tumor microenvironment drives dysfunction in intrapancreatic CD8 + T cells. J Exp Med 2020; 217.
24. Zhang YN, Song J, Wang H, Wang H, Zeng M, Zhai GT, et al. Nasal IL-4(+) CXCR5(+)CD4(+) T follicular helper cell counts correlate with local IgE production in eosinophilic nasal polyps. J Allergy Clin Immunol. 2016;137:462–73.

25. Yan B, Lou H, Wang Y, Li Y, Meng Y, Qi S, et al. Epithelium-derived Cystatin SN enhances eosinophil activation and infiltration through IL-5 in patients with chronic rhinosinusitis with nasal polyps. J Allergy Clin Immunol. 2019;144:455–69.
26. Muniz VS, Silva JC, Braga YAV, Melo RCN, Ueki S, Takeda M et al. Eosinophils release extracellular DNA traps in response to Aspergillus fumigatus. J Allergy Clin Immunol 2018; 141:571– 85.e7.
27. Persson EK, Verstraete K, Heyndrickx I, Gevaert E, Aegerter H, Percier JM et al. Protein crystallization promotes type 2 immunity and is reversible by antibody treatment. Science 2019; 364.
28. Lu Y, Huang Y, Li J, Huang J, Zhang L, Feng J, et al. Eosinophil extracellular traps drive asthma progression through neuro-immune signals. Nat Cell Biol. 2021;23:1060–72.
29. Bettigole SE, Lis R, Adoro S, Lee AH, Spencer LA, Weller PF, et al. The transcription factor XBP1 is selectively required for eosinophil differentiation. Nat Immunol. 2015;16:829–37.
30. Kim HJ, Sim MS, Lee DH, Kim C, Choi Y, Park HS, et al. Lysophosphatidylserine induces eosinophil extracellular trap formation and degranulation: implications in severe asthma. Allergy. 2020;75:3159–70.
31. Fazlollahi F, Kongmanas K, Tanphaichitr N, Mallen-St Clair J, Gopen Q, Faull KF, et al. Lipidomic profiling of sinus mucosa from patients with chronic rhinosinusitis. Clin Transl Sci. 2015;8:107–15.
32. Stevens WW, Staudacher AG, Hulse KE, Carter RG, Winter DR, Abdala-Valencia H, et al. Activation of the 15-lipoxygenase pathway in aspirin-exacerbated respiratory disease. J Allergy Clin Immunol. 2021;147:600–12.
33. Szatkowski P, Gielicz A, Stępień A, Hartwich P, Kacorzyk R, Plutecka H, et al. Unique effect of aspirin on local 15-oxo-eicosatetraenoic acid synthesis in asthma patients with aspirin hypersensitivity. Clin Transl Allergy. 2024;14:e70004.
34. Tyrak KE, Pajdzik K, Jakieła B, Kupryś-Lipińska I, Ćmiel A, Kacorzyk R, et al. Biomarkers for predicting response to aspirin therapy in aspirin-exacerbated respiratory disease. Clin Exp Allergy. 2021;51:1046–56.
35. Mastalerz L, Trąd G, Szatkowski P, Ćmiel A, Gielicz A, Kacorzyk R, et al. Aspirin hypersensitivity diagnostic index (AHDI): in vitro test for diagnosing of N-ERD based on urinary 15-oxo-ETE and LTE(4) excretion. Allergy. 2025;80:534–44.
36. Li Z, Zeng M, Deng Y, Zhao J, Zhou X, Trudeau JB, et al. 15-Lipoxygenase 1 in nasal polyps promotes CCL26/eotaxin 3 expression through extracellular signal-regulated kinase activation. J Allergy Clin Immunol. 2019;144:1228–e419.
37. Sim MS, Kim HJ, Bae I, Kim C, Chang HS, Choi Y, et al. Calcium ionophore-activated platelets induce eosinophil extracellular trap formation. Allergol Int. 2023;72:466–76.
38. Williams TL, Rada B, Tandon E, Gestal MC. NETs and EETs, a whole web of mess. Microorganisms 2020; 8.
39. Pathinayake PS, Waters DW, Nichol KS, Brown AC, Reid AT, Hsu AC, et al. Endoplasmic reticulum-unfolded protein response signalling is altered in severe eosinophilic and neutrophilic asthma. Thorax. 2022;77:443–51.
40. Kim YM, Jin J, Choi JA, Cho SN, Lim YJ, Lee JH, et al. Staphylococcus aureus enterotoxin B-induced Endoplasmic reticulum stress response is associated with chronic rhinosinusitis with nasal polyposis. Clin Biochem. 2014;47:96–103.
41. Sule G, Abuaita BH, Steffes PA, Fernandes AT, Estes SK, Dobry C et al. Endoplasmic reticulum stress sensor IRE1α propels neutrophil hyperactivity in lupus. J Clin Invest 2021; 131.
42. Pazdrak K, Moon Y, Straub C, Stafford S, Kurosky A. Eosinophil resistance to glucocorticoid-induced apoptosis is mediated by the transcription factor NFIL3. Apoptosis. 2016;21:421–31.
43. Milara J, Peiró T, Armengot M, Frias S, Morell A, Serrano A, et al. Mucin 1 downregulation associates with corticosteroid resistance in chronic rhinosinusitis with nasal polyps. J Allergy Clin Immunol. 2015;135:470–6.
44. Li Y, Chang LH, Huang WQ, Bao HW, Li X, Chen XH, et al. IL-17A mediates pyroptosis via the ERK pathway and contributes to steroid resistance in CRSwNP. J Allergy Clin Immunol. 2022;150:337–51.
45. Wen W, Liu W, Zhang L, Bai J, Fan Y, Xia W, et al. Increased neutrophilia in nasal polyps reduces the response to oral corticosteroid therapy. J Allergy Clin Immunol. 2012;129:1522–e85.
46. Ono E, Lenief V, Lefevre MA, Cuzin R, Guironnet-Paquet A, Mosnier A, et al. Topical corticosteroids inhibit allergic skin inflammation but are ineffective in impeding the formation and expansion of resident memory T cells. Allergy. 2024;79:52–64.
47. Okano M, Fujiwara T, Yamamoto M, Sugata Y, Matsumoto R, Fukushima K, et al. Role of prostaglandin D2 and E2 terminal synthases in chronic rhinosinusitis. Clin Exp Allergy. 2006;36:1028–38.
48. Gazi L, Gyles S, Rose J, Lees S, Allan C, Xue L, et al. Delta12-prostaglandin D2 is a potent and selective CRTH2 receptor agonist and causes activation of human eosinophils and Th2 lymphocytes. Prostaglandins Other Lipid Mediat. 2005;75:153–67.
49. Nordström A, Jangard M, Ryott M, Tang X, Svedberg M, Kumlin M. Mucosal LTE(4), PGD(2) and 15(S)-HETE as potential prognostic markers for polyp recurrence in chronic rhinosinusitis. Prostaglandins Other Lipid Mediat. 2024;174:106886.

Publisher's note